Holey SIW Horn Antenna Based on an H-plane Lens-wise Wavefront Collimation

SUBMISSION DATE / POSTED DATE

12-10-2022 / 17-10-2022

CITATION

Biedma-Pérez, Andrés; Padilla, Pablo; Segura-Gómez, Cleofás; Palomares-Caballero, Ángel (2022): Holey SIW Horn Antenna Based on an H-plane Lens-wise Wavefront Collimation. TechRxiv. Preprint. https://doi.org/10.36227/techrxiv.21316668.v1

DOI

10.36227/techrxiv.21316668.v1

This work has been accepted for publication in *IEEE Transactions on Antennas and Propagation*. DOI: 10.1109/TAP.2022.3210692

Holey SIW Horn Antenna Based on an H-plane Lens-wise Wavefront Collimation

Andrés Biedma-Pérez, Pablo Padilla, Cleofás Segura-Gómez, and Ángel Palomares-Caballero

***Abstract*—This paper presents an H-plane SIW horn antenna whose directivity is enhanced using holey unit cells along the horn flaring. By wisely drilling the horn antenna, it is possible to reduce the phase error in the aperture which is a common problem in horn antennas if the optimum dimensions are not employed. An analysis of the distribution of the unit cells along the horn antenna has been carried out to achieve the desired equivalent refractive indices. By changing the hole radius, different equivalent refractive indices can be tuned with a wideband performance. This fact enables the implementation of a collimation zone inside the horn antenna which transforms the pseudo-circular wavefront into a quasi-planar one in the radiating aperture. The produced directivity is similar to the horn antenna with the optimum dimensions but a longitudinal reduction of 53.7% and a higher realized gain are achieved. A holey SIW horn antenna is designed and manufactured. The measured results show an impedance bandwidth performance below -10 dB from 34.3 GHz to 44.5 GHz (25.9%) with a realized gain above 10 dBi. The gain difference regarding a SIW horn antenna without the collimation zone is about 2-3 dBi in the operating frequency range.**

***Index Terms*—Antenna aperture, holey unit cell, horn antenna, phase front correction, substrate integrated waveguide (SIW).**

I. Introduction

THE horn antenna is a type of aperture antenna that has been widely used due to its capability to provide high directivity in a wide bandwidth with a simple antenna design [1]. One of the main problems with horn antennas is the non-uniform phase distribution in the radiating aperture. This entails a decrease in the aperture efficiency and in consequence, in the maximum directivity that can be provided. Several design strategies have been presented in the literature to reduce this phase unbalance in the aperture. In work [2], a planar dielectric lens has been inserted after the horn antenna to correct the non-uniform phase distribution in the horn aperture. As an alternative to the use of lenses, metasurfaces have been proposed in [3], [4] to achieve the same phase correction. Exotic metamaterials have also been employed around the horn aperture to enhance this phase distribution [5]. In contrast to the previous solutions, [6] presents a rectangular horn with an improved aperture efficiency by the optimized sizes of the rectangular waveguide discontinuities along the horn profile.

With the appearance of waveguide planar solutions such as substrate integrated waveguide (SIW) [7], H-plane horn antennas have been the focus of attention in recent years. Similar to the solutions presented above for conventional waveguide horn antennas, some works have adapted these design approaches to H-plane horn antennas. In [8], a dielectric lens has been placed after the horn aperture to reduce the beamwidth. For a silicon substrate horn antenna presented in [9], different sizes of holes are inserted after the flaring to effectively implement a lens. On the other hand, [10] and [11] set the optimum dimensions for a H-plane horn antenna and enhance the magnitude distribution in its aperture by implementing hard boundary conditions in the lateral walls.

More compact solutions have been recently reported to tackle the phase error problem of H-plane horn antennas. The idea lies in implementing structures that correct this phase error along the horn flaring, where the phase error occurs, instead of after the horn aperture. In this way, the compactness of the antenna design is considerably increased. Some H-plane horn designs that insert phase-correction elements along the horn flaring are in the literature. In the design presented in [12], the correction of the phase distribution in the aperture is achieved by embedded metal vias which modify the phase velocity in some areas of the horn flaring. An improvement in terms of impedance bandwidth is shown in [13] where the tuning of the phase velocity is carried out by slanted slots along the SIW horn. Another recent design strategy to provide uniformity in the phase distribution of H-plane horns is the use of slow-wave (SW) structures which reduce the phase velocity as opposed to the previous mentioned approaches. These SW structures have been implemented in conventional rectangular waveguide for H-plane horns as metal pins [14], [15] and for SIW horns as metallized blind via-holes [16]. A combination of structures that produce lower and higher phase velocity by using embedded vias and air hole arrays, respectively, is presented in [17] but for a tapered slot antenna.

The antenna design proposed in this paper presents an improvement in terms of operating bandwidth and cost-effectiveness of the aforementioned H-plane SIW horns. By the use of holey unit cells along the horn flaring, a collimation zone is implemented allowing the phase front correction in a easy and effective way for a wideband frequency range. Since the proposed unit cells contain air holes, they tend to reduce the phase constant as the radius of the holes increases, which is an alternative solution to the performance obtained with SW structures [14]–[16].

II. Lens-wise H-plane field collimation model

Our H-plane SIW horn antenna design is based on the idea of adding the field collimation effect along the horn flaring. The area in which the collimation occurs transforms the pseudo-circular wavefront inside the horn into a quasi-planar wave in the aperture of the horn. As a consequence, this zone provides a lens behaviour inside the horn, which is a compact design compared to the case of using a lens-type structure after the horn aperture.

The conventional SIW technology provides a fixed substrate permittivity for the wave propagation. There are different strategies in which the lens effect can be introduced in the SIW horn antenna, all of them related to the proper modification of the phase constant along the horn flaring. Regarding the approaches reported in the literature to achieve this aim, embedded metal vias [12], [16] and slanted slots [13] are proposed for the SIW horn antennas. Nevertheless, these solutions suffer from poor bandwidth for what is expected of a horn antenna [12], [16] or, they are based on modified waveguides implemented in the horn [12], [13] for which the design procedure is not as straightforward as the proposed one. Here, we present the

This work was supported in part by the Spanish Government under Project PID2020-112545RB-C54 and, Project RTI2018-102002-A-I00, in part by "Junta de Andalucía" under Project B-TIC-402-UGR18, Project A-TIC-608-UGR20, Project PYC20-RE-012-UGR and Project P18.RT.4830, and in part by the Predoctoral Grants FPU20/00256 and FPU18/01965.

A. Biedma-Pérez, P. Padilla, C. Segura-Gómez, and Á. Palomares-Caballero are with the Department of Signal Theory, Telematics and Communications, Universidad de Granada, 18071 Granada, Spain. (email: abieper@correo.ugr.es; pablopadilla@ugr.es; cleofas@ugr.es; angelpc@ugr.es)

design of a collimation zone based on holey unit cells of different radius values. The simplest configurations for the collimation zone in terms of the characterization of the electromagnetic behaviour are the ones based on: cartesian distribution (x, y), pure radial distribution (r, θ) or a mixed distribution with the r location fixed to columns in x and uniform angular distribution in θ (x, θ). These three options are displayed in Fig. 1. Each of these three different regular grid distributions have their own particularities. The first option, the cartesian grid (see Fig. 1(a)), is the easiest one in terms of the calculation of its electromagnetic behaviour considering the periodic eigenmode analysis of the holey unit cell of size [p_x, p_y]. The geometric details of the proposed unit cell for the 2D periodic grid are provided in the inset of Fig. 2(a). The top view of the unit cell and the zone under analysis are illustrated. The black colored area represents the substrate and the hole (air) is placed in the middle of the unit cell. In the z-direction, a perforated perfect electric conductor (PEC) surface is located on both the top and bottom of the unit cell. In addition, air blocks outside the unit cell have been included to emulate open conditions when the dispersion diagram is computed by the eigensolver of the CST Studio Suite. The computation of the dispersion diagram of the unit cell provides the phase constant value k_x related to frequency. With this relation, it is straightforward to obtain the refractive index versus frequency for any propagation direction and any radius value in the available range (for instance, $0.05p/2$ to $0.95p/2$ for a square unit cell, considering possible manufacture constraints). Figure 2(a) provides the dispersion diagram for a rectangular holey unit cell, along with the inherent relation of the equivalent refractive index (n) with the frequency, provided in Fig. 2(b). The behavior of n along the frequency is approximately constant except when the frequency is close to 45 GHz. This is because for larger hole radii, in $k_x p = 180^{\circ}$, the frequency is lower due to the increase of the bandwidth of the stopband which appears when the unit cell is drilled. Moreover, we can see that, as the radius increases, the refractive index decreases because there is less dielectric in the unit cell. In the first regular grid distribution, since the horn structure has a radial geometry, the ray tracing inside the horn does not follow the cartesian grid. This means that every hole of the grid must have its own radius value according to the desired phase constant value at this point of the grid, increasing the complexity of the grid design. The second option (see Fig. 1(b)) provides a radial distribution that suits the radial horn geometry, at the expense of not being directly analyzable with the eigensolver because the edges of the unit cell are not parallel to the periodic directions. The third option (see Fig. 1(c)) is a mixture which keeps the advantages of the previous two: radial distribution in the propagation direction, which implies that it is needed the same refraction index value for any hole in a particular radial row, with an equal distributions in columns in the x-direction where the centers of the holes of the same columns are aligned. This option also permits the structure analysis considering the unit cell, as it is detailed in the next section.

III. Holey SIW unit cell for refractive index variation

The proposed holey unit cell is the one depicted in the inset of Fig. 2(a). The initial size of the rectangular unit cell is set to have p_x = 1.7 mm and p_y = 1.3 mm. With these dimensions and considering a center frequency at 40 GHz, the horn antenna is decided to be designed around the upper limit in the operating bandwidth of the unit cell.

When the mixed distribution option is examined, it can be recognized that: i) the unit cell deforms its rectangular shape as the radial row angle increases, and ii) the y (p_y) dimension of the unit cell is increased for the different columns, while the x dimension (p_x) remains unaltered. The first issue can be neglected by selecting an

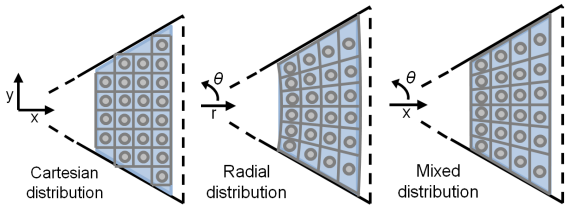

Fig. 1. Hole distribution options in the collimation zone of the SIW horn antenna: (a) cartesian distribution (x, y), (b) radial distribution (r, θ), and (c) mixed distribution with r fixed to columns in x and uniform angular distribution in θ (x, θ)

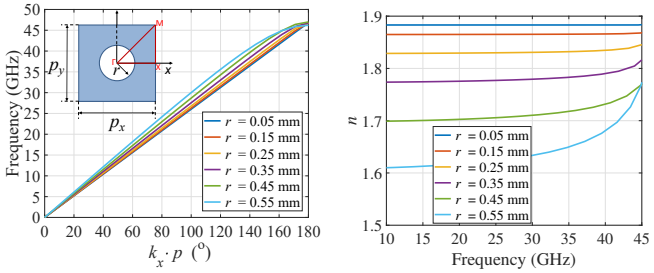

Fig. 2. Holey unit cell: (a) Example of the dispersion diagram of the irreducible $\Gamma - X - M$ Brillouin zone for a rectangular holey unit cell with dimensions: p_x = 1.7 mm and p_y = 1.3 mm and r = 0.05 to 0.55 mm, and (b) relation of the equivalent refractive index (n) with the frequency.

equivalent rectangular unit cell, as it is depicted in Fig. 3(a). The second issue has to be carefully considered when the structure is analyzed. The analysis of the complete structure can be carried out with the dispersion diagram analysis of the equivalent rectangular unit cell. By rotating the equivalent rectangular unit cell to align it with the radial row and therefore, the propagation direction is aligned with the horizontal main axis of the unit cell (x') as it is presented in Fig. 3(b). This case is quite useful since the vertical main axis of the unit cell (y') is orthogonal to the propagation direction, and the size variation p_y has negligible effect in the unit cell behaviour along the x' direction as it is demonstrated in Fig. 4. Additionally, the equivalent unit cell has to be enlarged to the new p_x value that is $p'_x = p_x/cos(\theta)$. Thus, the design of each radial row can be done by analyzing the equivalent rectangular rotated unit cell only along its x' direction and for its appropriate p'_x value. This is the approach selected for our design.

The design of the collimation zone is, in fact, reduced to the calculation of the propagation behaviour of each radial row. The selection of the refractive index of each radial row is derived from a geometrical problem analyzed by ray tracing: the different phase delay values in the aperture, due to the length of each row to the aperture, are compensated by the wave acceleration introduced in each row. This yields a uniform phase distribution in the aperture and a planar wavefront in the steering direction. Therefore, since the holey unit cells of each radial row are identical, each row design can be obtained by analyzing the equivalent rectangular rotated unit cell along its x' direction and for its appropriate p'_x value, neglecting the variations in the p'_y dimension. Fig. 5 provides the results of different equivalent refractive index values when a radial row is set. This implies a θ value which has to be considered in the equivalent holey unit cell. As can be seen, the values of n are different depending on the chosen radial row, being more evident this difference for larger values of the radius of the holes. Therefore, the equivalent holey unit

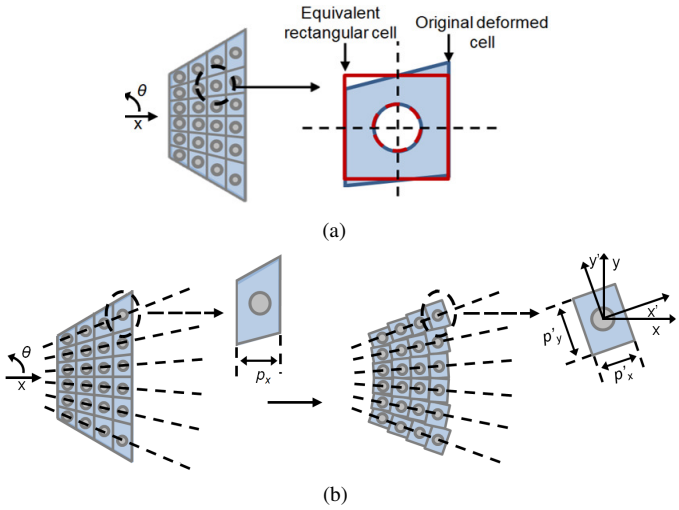

Fig. 3. Unit cell analysis selection for the mixed distribution: (a) equivalent rectangular unit cell for deformed unit cells and, (b) dispersion diagram analysis considering unit cell rotation to fix the propagation direction aligned with the radial row, and $p'_x = p_x/cos(\theta)$.

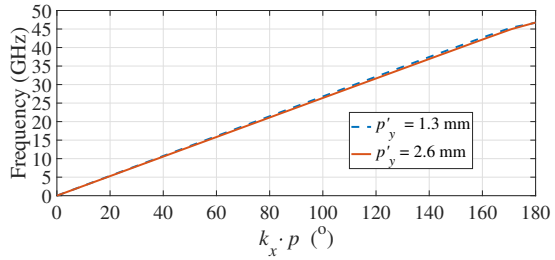

Fig. 4. Dispersion diagrams for the x' propagation direction when the p'_y dimension is varied (r = 0.25 mm, p'_x = 1.7 mm, p'_y = 1.3 to 2.6 mm).

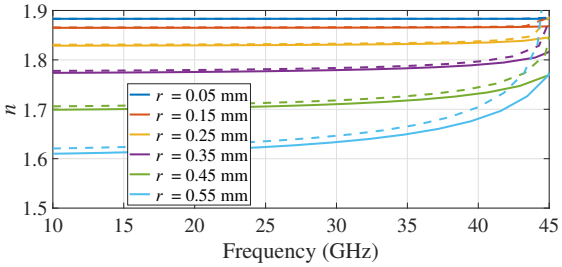

Fig. 5. Range of the equivalent refractive index values available for the holey unit cell by modifying radius value: (a) for a radial row whose $\theta = 0^o$ (solid line) and thus, $p'_x = p_x$, (b) for a radial row $\theta = 22^o$ (dashed line) and thus, $p'_x = p_x/cos(22^o)$.

cell are needed for an accurate design of the collimation zone depicted in the next section. It is important to note that for the implementation of the collimation zone by the holey unit cells, holes with radius greater than 0.45 mm will be avoided. This is because the equivalent refractive index is not stable enough in the considered frequency range. Besides, this limit set for the radius of the holes ensures a low level of reflection in the holey unit cell along the frequency.

IV. Complete SIW horn antenna design

The complete horn design pursues the reduction of the H-plane beamwidth and the increase of the directivity. If no phase front correction is added, a wide horn aperture and angular widening would result in a higher phase error in the aperture and a low directivity as a consequence. However, the phase front correction produced by the collimation zone offers an increase of the directivity in the H-plane. The SIW horn antenna is designed using RO4003C substrate, with a relative permittivity (ε_{SIW}) of 3.55 and tabulated loss tangent $tan\delta$ of 0.0027 at 10 GHz. The proposed H-plane SIW horn antenna has three main parts: the feeding interface, the collimation zone and the transition to the air. The main part is the collimation zone that enhances phase front in the aperture of the horn antenna to increase its directivity. The three parts are described in the following subsections. Notice that the proposed configuration only provides a highly directive radiation beam in the H-plane, while the broad nature of the E-plane beamwidth is preserved.

A. Collimation zone design

The proper definition of the collimation zone and its features is the key in the complete design. Since a plane phase front in the SIW horn aperture is the desired goal, a geometrical analysis of the structure can be carried out. The difference of distance from the equivalent focal point at the waveguide-to-horn transition to the horn aperture among the different angular paths is translated into a phase difference. As a consequence, there is a phase error from the center of the aperture to any other angular path. Therefore, if the phase constant distribution in the normal plane to the propagation direction is tuned adequately, the phase error can be severely reduced and every angular path has the same electrical distance to the horn aperture. Fig. 6 illustrates the geometrical insight of the horn design and the collimation zone.

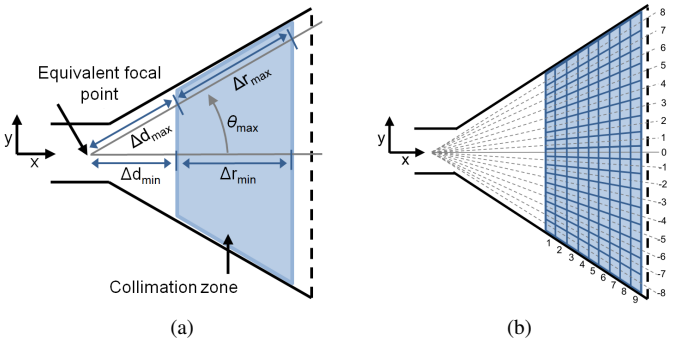

Fig. 6. Collimation zone: (a) geometrical analysis for the phase correction, (b) angular configuration of the unit cells.

The phase correction needed is derived from the geometric analysis:

$$phase = \frac{2\pi}{\lambda_0}(n_r \Delta r + n_d \Delta d), \quad (1)$$

where λ_0 is the vacuum wavelength, n_r and n_d are the refraction index values along the path, and Δr + Δd are the distances along the path, for the the two different zones. If the electrical distance at any angular path is forced to be the same, the geometrical relation implies:

$$\frac{2\pi}{\lambda_0}(n_{r\,min}\Delta r_{min} + n_d \Delta d_{min}) = \frac{2\pi}{\lambda_0}(n_r \Delta r + n_d \Delta d), \quad (2)$$

where n_d = $n_{r\,min}$ is the refraction index value inside the SIW substrate, n_{SIW}, which yields the maximum refraction index value, $n_{max} = n_d$. Then, for any angular path (θ), the desired refraction index is computed as:

$$n_\theta = \frac{n_{SIW}(\Delta r_{min} + \Delta d_{min} - \Delta d)}{\Delta r}. \quad (3)$$

If the angular dependence between paths is included, the desired refraction index is:

$$n_\theta = n_{SIW}\left(cos\theta - \frac{\Delta d_{min}}{\Delta r_{min}}(1 - cos\theta)\right). \quad (4)$$

Thus, the design of the collimation zone implies the definition of the refraction index value distribution in the normal plane to the propagation direction. Fig. 7 provides the desired refractive index distribution for the H-plane SIW horn. The profile of the refractive index with respect to θ is similar to that obtained for gradient index (GRIN) lenses [2].

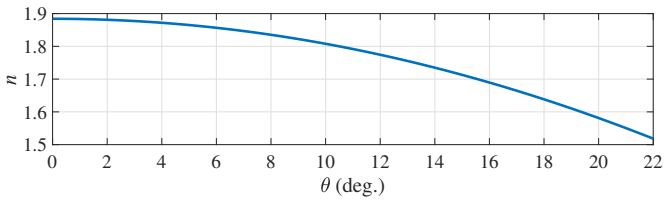

Fig. 7. Refraction index distribution in the normal plane to the propagation direction, for $\theta_{max} = 22^o$, $\Delta d_{min} = 25$ mm, $\Delta r_{min} = 15$ mm and $\varepsilon_{SIW} = 3.55$.

These refractive index values according to the angular path can be related to the ones provided by the unit cell. Based on the required refractive indices and those achieved for the holey unit cell, a partial phase correction is expected for the larger angular paths. The collimation zone presented in Fig. 6(b) is divided into a mixed distribution of unit cells, with reference size of $d_x = 1.7$ mm and $d_y = 1.3$ mm, for 9 columns, $N_y = [1:9]$ and 17 equivalent angular paths, N_x = [-8:1:8]. Fig. 6(b) provides the angular design scheme. The electromagnetic simulations have been performed with CST Studio Suite. Fig. 8 shows the simulated results for the normalized phase and magnitude distributions in the aperture for different horn antenna designs. The performance comparison include the SIW horn antenna with the collimation zone, the same horn design but without collimation zone and the optimum horn antenna whose aperture has the same size as the previous ones but its length is the optimum at 40 GHz [1]. The normalized phase distributions at different frequencies reveal a phase front correction similar or even better than the one obtained in the optimum case. This proves the proper performance of the proposed holey unit cell. For aperture positions y further away from the center, a partial phase correction is achieved due to the frequency behaviour of the holey unit cell for large radii. Regarding the magnitude distributions in Fig. 8(d), the case with collimation zone is narrower than the other cases due to the presence of holes along the horn flaring. The expected consequence of this narrowing in the magnitude distribution is a decrease of the side lobe level [18]. For all the horn designs, the magnitude distribution has a cosine form because the excitation comes from the fundamental mode of the SIW, which is a TE_{10}. Therefore, since the magnitude is very low at the edges of the horn aperture, no unit cells have been implemented in the ± 8 angular paths (see Fig. 6(b)).

B. Complete antenna design and transitions

The complete antenna design is illustrated in Fig. 9. To feed the proposed SIW H-plane horn, a transition from a coaxial to SIW technology is employed, as it can be seen in the inset of Fig. 9. This transition design achieves a wideband transmission from the coaxial connector to the SIW in millimeter-wave frequencies, transforming the fundamental mode of the coaxial line (TEM mode) into the fundamental mode of the waveguide (TE_{10} mode). On the other hand,

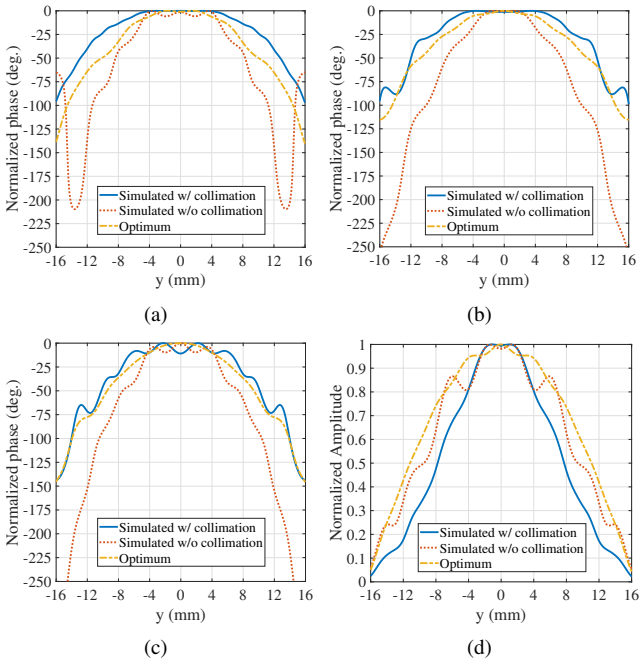

Fig. 8. Normalized phase distribution in the aperture of each horn antenna design at: (a) 36 GHz, (b) 40 GHz and, (c) 44 GHz. (d) Normalized magnitude distribution in the aperture at 40 GHz.

a transition composed of the same dielectric slab with four metallized - non-metallized strips is included after the horn aperture [19]. This transition is able to match the refractive indices shown in Fig. 7 to the free space as if it were a matching layer for a GRIN lens. Additionally, some small radius holes have been introduced in the larger angular paths to improve their matching at the beginning of the collimation zone. It is important to note that due to the subwavelength size of the holes implemented in the collimation zone, there are negligible radiation losses along the flaring horn. The maximum radiation losses are produced by the holey unit cell with the greatest radius and they are around 0.013 dB.

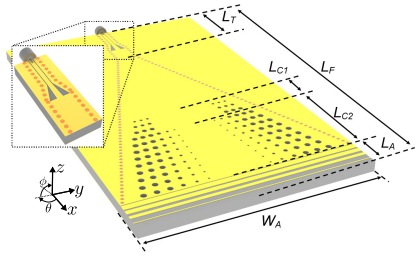

Fig. 9. 3D view of the proposed horn antenna. The dimensions are: L_T = 11.7, L_{C1} = 4.3, L_{C2} = 15, L_A = 5.3, and W_A = 34.5, and L_F = 57. All dimensions are in mm.

V. Prototype and Measurement Results

The final design of the complete H-plane SIW horn antenna is manufactured in order to validate the proper device performance. The commercial connector used is an end-launch connector (91R60918) with a 1.85 mm 50 Ω coaxial port. Fig. 10 shows the prototype, along with the measurement setup for its characterization. The measurements have been carried out at the antenna measuring facilities of the University of Granada (SWT Lab).

The measured results of the reflection coefficient $|S_{11}|$ are illustrated in Fig. 11 including the comparison with the simulated results.

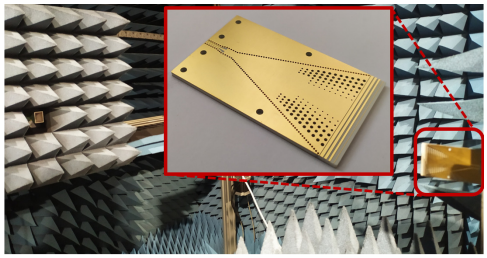

Fig. 10. Antenna prototype and measurement setup.

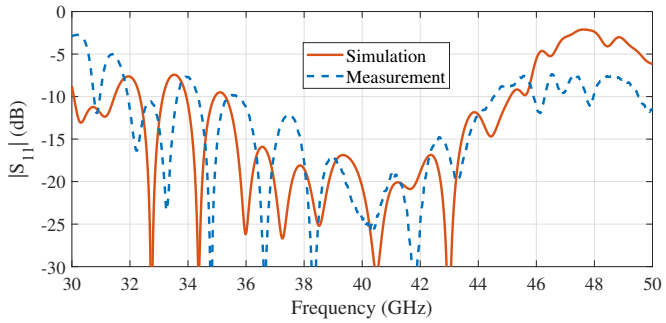

Fig. 11. $|S_{11}|$ measurement result compared to the simulation one.

The measured working band is in accordance with the designed one and only a slight differences are observed. The obtained operating band in terms of impedance matching ranges from 34.3 GHz to 44.5 GHz. The radiation patterns of the proposed horn antenna and compared the SIW horn designs of Fig. 8 are shown in Fig. 12. The H-plane radiation patterns (XY plane) of the horn with collimation zone are very similar to the ones obtained with the optimum horn design. It is also observed how the beamwidth is widened for the case without collimation zone, resulting in a loss of directivity. For the E-plane (XZ plane), similar radiation patterns are obtained among all the horn designs since they have the same dielectric thickness. Some ripples appear in positive θ in the simulated and measured E-plane radiation patterns. This is produced by the radiation of the grounded coplanar-waveguide included in the transition of the input port. In the H-plane radiation patterns of the horn antenna without collimation zone, it appears some ripples in the main beam for other frequencies due to the phase and magnitude distributions arriving at the aperture. The cross polarization of the proposed horn antenna has also been measured, the obtained results reveal a maximum level of -30 dB in the operating band.

The directivity and realized gain of the proposed horn antenna are displayed in Fig. 13. In this figure, it is also included the simulated results for the horn antenna without the collimation zone and the optimum one. Both directivity and realized gain values are corresponding to the direction of maximum radiation, that is, the direction of maximum radiation: $(\phi, \theta) = (0^o, 0^o)$. The directivity of the horn antenna with collimation zone is similar to the one produced by the optimum horn antenna. This is expected because of the similarity in their radiations patterns observed in Fig. 12. However, in the realized gain results, we observe higher realized gain for the proposed horn antenna because of two main reasons: i) a shorter distance of the horn flaring; and ii) the holey unit cells introduced along the horn flaring replace dielectric by air. These two facts reduce the amount of losses due to the dielectric material originated when the wave propagates along the SIW horn. Therefore, the radiation efficiency of the optimum horn is lower than the one of the proposed horn and hence the realized gain. In addition to this improvement,

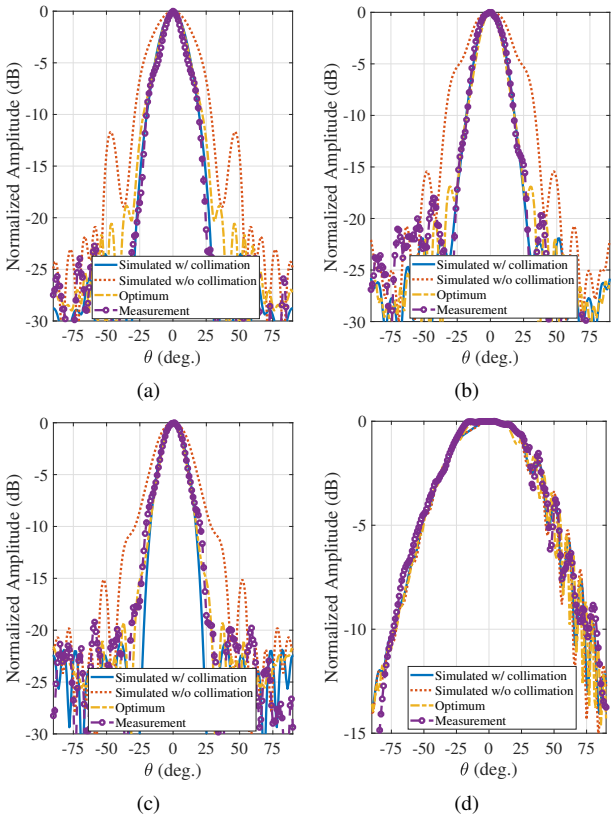

Fig. 12. Radiation patterns: in the H-plane at (a) 36 GHz, (b) 40 GHz and, (c) 44 GHz. (d) In the E-plane at 40 GHz.

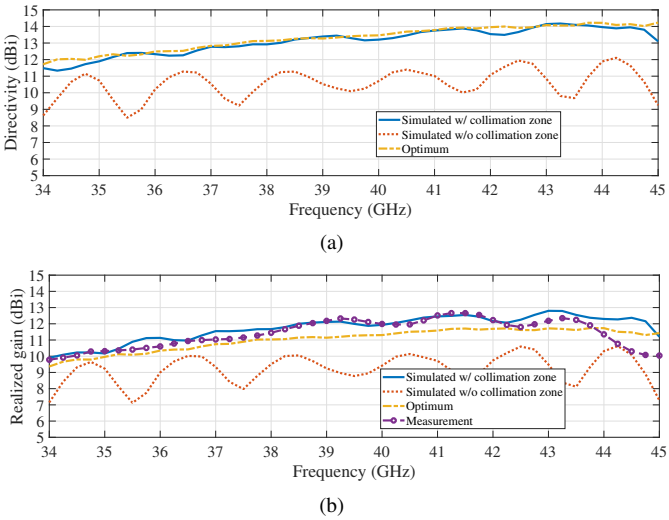

Fig. 13. (a) Directivity and (b) realized gain results in the working frequency range.

it is achieved a 53.7% reduction regarding the longitudinal length of the optimum horn antenna. The aperture efficiency of the horn with collimation zone has been calculated using the formula proposed in [20]. The traditional formula is above 1 for this horn antenna because the transition used after the aperture of the horn antenna. The obtained aperture efficiency is between 0.45 and 0.6 in the operating bandwidth.

Finally, Table I presents a performance comparison between the proposed holey SIW H-plane horn antenna and other works of H-plane horn antenna designs where the phase front along the horn

TABLE I
COMPARISON BETWEEN THE RELATED H-PLANE HORN ANTENNAS WITH INTEGRATED PHASE-CORRECTION STRUCTURES

Ref.	Frequency band (GHz)	Technology	Design approach	Average gain increase (dBi)
[12]	35.5	SIW	Ray tracing & embedded WG	2.3
[13]	32-38.5 (18.4%)	SIW	Ray tracing & embedded WG	2
[16]	26.5-29.5 (10.71%)	SIW	Optimization & SW structures	2.7
[14]	26-40 (42.4%)	Standard waveguide	Optimization & SW structures	0.8 (26-33 GHz) 1.7 (33-40 GHz)
[15]	10.5-14.5 (32%)	Standard waveguide	Optimization & SW structures	1.7
[21]	12-16 (28.6%)	Standard waveguide	Transformation optics	1.9
This work	34.3-44.5 (25.9%)	SIW	Ray tracing & collimation zone	2.3

flaring is corrected. From this table, the proposed design approach offers a substantial increase in operating bandwidth for SIW H-plane horn antennas. Horn designs based on standard waveguide technology are expected to have a wider operating bandwidth due to the non-use of dielectrics in their structure, which facilitates the employed transitions for both feeding and radiation in the horn aperture. However, the cost of implementation of the phase-correction structures is higher as they do not allow monolithic designs and the manufacturing has to be done in two separate layers. Regarding the strategy to design the phase-correction structures inside the horn flaring, the proposed one relies on ray tracing and a collimation zone based on unit cells with wideband performance. In contrast to this design strategy, most of the reported horn designs are based on the optimization of the phase-correction structures inside the horn flaring or based on embedded waveguides (WG) which offer a lower operating bandwidth. The presented design strategy is more straightforward, offers greater bandwidth and low implementation cost with an average gain increase similar to designs reported in the literature.

VI. CONCLUSION

In this work, a holey SIW H-plane horn antenna is presented as a low-complex solution to correct phase error that occurs in SIW horn antennas. By simply drilling the horn antenna with the required hole distribution, a collimation zone can be implemented along the horn flaring. The implemented holey unit cells produce different equivalent refraction index that allow a phase front correction inside the antenna over a wide frequency range. This fact yields to an average gain increase of 2.3 dBi regarding a conventional SIW H-plane horn antenna without collimation zone. The proposed SIW horn design also presents a higher realized gain than that obtained with the optimum horn design for the same aperture size. This fact is achieved with a longitudinal length reduction of 53.7% regarding the optimum horn design. A prototype is manufactured and the measured results reveal a wide impedance bandwidth from 34.3 GHz to 44.2 GHz with a gain above 10 dBi in the operating frequency range.

REFERENCES

[1] C. A. Balanis, *Antenna theory: analysis and design*, 4th ed. New York, NY, USA: Wiley, 2016.

[2] M. K. T. Al-Nuaimi, W. Hong and Y. Zhang, "Design of high-directivity compact-size conical horn lens antenna," *IEEE Antennas Wireless Propag. Lett.*, vol. 13, pp. 467-470, 2014.

[3] Y. He, N. Ding, L. Zhang, W. Zhang and B. Du, "Short-length and high-aperture-efficiency horn antenna using low-loss bulk anisotropic metamaterial," *IEEE Antennas Wireless Propag. Lett.*, vol. 14, pp. 1642-1645, 2015.

[4] K. Liu, Y. Ge and C. Lin, "A Compact Wideband High-Gain Metasurface-Lens-Corrected Conical Horn Antenna," *IEEE Antennas Wireless Propag. Lett.*, vol. 18, no. 3, pp. 457-461, March 2019.

[5] D. Ramaccia, F. Scattone, F. Bilotti and A. Toscano, "Broadband compact horn antennas by using EPS-ENZ metamaterial lens," *IEEE Trans. Antennas Propag.*, vol. 61, no. 6, pp. 2929-2937, June 2013.

[6] T. S. Bird and C. Granet, "Optimization of profiles of rectangular horns for high efficiency," *IEEE Trans. Antennas Propag.*, vol. 55, no. 9, pp. 2480-2488, Sept. 2007.

[7] K. Wu, M. Bozzi and N. J. G. Fonseca, "Substrate integrated transmission lines: review and applications," *IEEE Journal of Microwaves*, vol. 1, no. 1, pp. 345-363, Jan. 2021.

[8] H. Wang, Da-Gang Fang, B. Zhang, and Wen-Quan Che, "Dielectric loaded substrate integrated waveguide (SIW) H-plane horn antennas", *IEEE Trans. Antennas Propag.*, vol. 58, no. 3, March 2010.

[9] J. Liang, W. Gao, H. Lees and W. Withayachumnankul, "All-silicon terahertz planar horn antenna," *IEEE Antennas Wireless Propag. Lett.*, vol. 20, no. 11, pp. 2181-2185, Nov. 2021.

[10] N. Bayat-Makou and A. A. Kishk, "Substrate integrated horn antennas with improved aperture efficiency," in *2017 XXXIInd General Assembly and Scientific Symposium of the International Union of Radio Science (URSI GASS)*, 2017.

[11] N. Bayat-Makou and A. A. Kishk, "Substrate integrated horn antenna with uniform aperture distribution," *IEEE Trans. Antennas Propag.*, vol. 65, no. 2, pp. 514-520, Feb. 2017.

[12] L. Wang, X. Yin, S. Li, H. Zhao, L. Liu and M. Zhang, "Phase corrected substrate integrated waveguide H-plane horn antenna with embedded metal-via arrays," *IEEE Trans. Antennas Propag.*, vol. 62, no. 4, pp. 1854-1861, April 2014.

[13] L. Wang, Esquius-Morote H. Qi, X. Yin, and J. R. Mosig. "Phase corrected H-plane horn antenna gap SIW technology", *IEEE Trans. Antennas Propag.*, vol. 65, no. 1, Jan. 2017.

[14] D. Sun and J. Xu, "Compact phase corrected H-plane horn antenna using slow-wave structures," *IEEE Antennas Wireless Propag. Lett.*, vol. 16, pp. 1032-1035, 2017.

[15] J. -Y. Deng *et al.*, "Horn antenna with miniaturized size and increased gain by loading slow wave periodic metal blocks," *IEEE Trans. Antennas Propag.*, vol. 69, no. 4, pp. 2365-2369, April 2021.

[16] Y. Zhang, J. -Y. Deng, D. Sun, J. -Y. Yin and L. -X. Guo, "Compact slow-wave SIW H-plane horn antenna with increased gain for vehicular millimeter wave communication," *IEEE Trans. Veh. Technol.*, vol. 70, no. 7, pp. 7289-7293, July 2021.

[17] Y. Yin, Q. Zhang, and S. Li, "Air and metal vias combined metamaterial-based lens for radiation performance enhancement of short-pulse tapered slot antenna," *Electronics*, vol. 10, no. 22: 2845, Nov. 2021.

[18] J. -Y. Deng, R. -Q. Luo, W. Lin, Y. Zhang, Z. Chen and L. -X. Guo, "Longitudinally miniaturized H-plane horn antenna with -30 dB sidelobes realized by simple blocks redistributing the aperture field," in *IEEE Trans. Antennas Propag.*, doi: 10.1109/TAP.2022.3164459.

[19] C. Segura-Gómez, Á. Palomares-Caballero, A. Alex-Amor, J. Valenzuela-Valdés and P. Padilla, "Modular design for a stacked SIW antenna array at Ka-Band," *IEEE Access*, vol. 8, pp. 158568-158578, 2020.

[20] L. Dai, Y. Xie, H. Wang, and P. Wu, "Three-dimensional aperture principle for end-fire radiation antenna array" *AIP Adv.*, vol. 11, no 2, p. 025116, 2021.

[21] H. Eskandari, J. L. Albadalejo-Lijarcio, O. Zetterstrom, T. Tyc, and O. Quevedo-Teruel, "H-plane horn antenna with enhanced directivity using conformal transformation optics," *Sci. Rep.*, vol. 11, no. 1, p. 14322, Jul. 2021.